International Journal of ISSI, Vol.3 (2006), No. 2, pp. 7-16

Mathematical Modeling of Heat Transfer for Steel Continuous Casting Process

M. Alizadeh[1*], H. Edris[2] and A. Shafyei[3]
1, 2, 3- Department of Materials Engineering, Isfahan University of Technology, Isfahan,8415683111, Iran
Received February 10, 2007; Accepted October 7, 2007

Abstract
Heat transfer mechanisms and the solidification process are simulated for a continuous casting machine and the geometric shape of the liquid pool is predicted considering different conditions. A heat transfer and solidification model is described for the continuous casting of steel slabs. The model has been established on the basis of the technical conditions of the slab caster in the continuous casting unit of Mobarakeh Steel Company. This model involves a two-dimensional (2-D) transient energy equation. The governing equation was solved using the finite-volume procedure. The boundary conditions of the mold, water spray cooling, and air cooling regions have been defined. The mathematical model is able to predict the shell thickness, temperature distribution in the mold and shell, and the interfacial gap between shell and mold. The modeling results were verified by the measured slab surface temperatures and a reasonable agreement was achieved.

Keywords: Heat transfer, Solidification, Continuous casting, Mathematical modeling.

Introduction

A continuous casting process setup is shown in Figure 1. Different regions of cooling in the continuous casting machine are shown in this figure. Since heat transfer plays an important role in continuous casting, it is desirable to have a quantitative understanding of the heat flow processes which will permit the prediction of the shell profile and temperature distribution as a function of the casting variables.

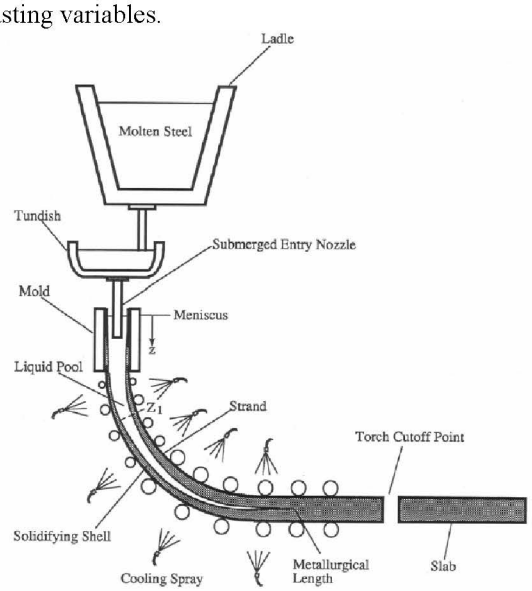

Fig. 1. Schematic of continuous casting process.

In the copper mold heat is transported to the cooling water. Below the mold, in the so-called secondary cooling zone, cooling is performed by water sprays, by contact with water cooled support rolls, and in the lower part of the machine, by radiation.

The mold must be able to extract sufficient heat from the incoming molten steel to solidify a shell which can support the liquid pool at the mold's exit, and thereby minimize breakouts. It is also important for the mold to be able to remove the heat uniformly to avoid the formation of thin regions in the shell which could rupture and lead to breakouts or surface cracks. Therefore, the mold provides support for the newly solidified steel shell at a time when the shell is weak and sensitive to bulging due to ferrostatic pressure [1].

Heat transfer in the mold region is controlled by: the convection of liquid superheat to the shell surface, latent heat evolution in the mushy zone, heat conduction through the solid shell, the thickness and other properties of the interface between the shell and the mold, heat conduction through the copper mold, and heat convection to the mold-cooling water [2].

The mechanism of heat transfer from the surface of the strand to the cooling water is complex. It involves resistances in the layer of flux or resolidified mold powder, in the air gap, the mold wall, and in the mold/cooling water interface.

* *Corresponding author:*
Tel: +98- 311- 3912750-1 Fax: +98- 311- 3912752
E-mail: alizadeh@ma.iut.ac.ir
Address: Dept. of Materials Engineering, Isfahan University of Technology, Isfahan, 8415683111, Iran

1. PhD student, Department of Materials Engineering, Isfahan University of Technology
2. Associate Professor, Department of Materials Engineering, Isfahan University of Technology
3. Assistant Professor, Department of Materials Engineering, Isfahan University of Technology

Table 1. Comparison of thermal conductivities of materials present in the continuous casting mold [3].

Materials	Temperature (°C)	Thermal conductivity ($W\ m^{-1}\ K^{-1}$)
Steel St 37	1200	29
Copper	30-130	385
Casting flux	1000-1300	0.5 to 1.2
Water	25	0.62
Radiation conductivity of gas gap	1000	0.043

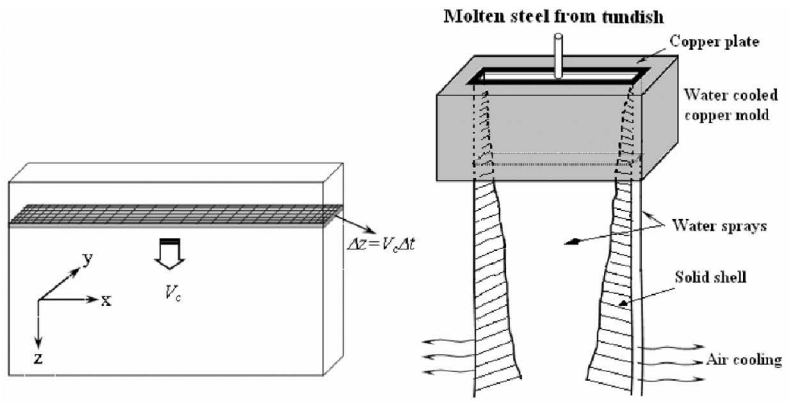

Fig. 2. Different regions and simulation domain in continuous casting process.

The thermal conductivities of different layers are compared in Table 1. As shown in this table, the air gap has the largest resistance to heat flow, while the other parts have a comparatively small resistance. Therefore, the pattern of heat removal in the mold is dependent largely upon the dynamics of gap formation. The air gap or contact resistances can be generated by the shrinkage of the steel shell away from the mold walls, especially after the flux is completely solid and unable to flow into the gaps. More researches were performed to show that the air gap was usually created in the lowest one-third of the mold length [3].

In the upper part of the secondary cooling zone, the strand is usually sprayed by water emerging from nozzles arranged in the spaces between the rolls. The rate at which heat is extracted from the strand surface by water sprays has been measured by many researchers. These researchers have shown that under normal continuous casting conditions, in which shell surface temperatures range between 700 and 1200 °C, surface temperature has a little effect on the heat transfer coefficient. All studies agree that, in the stated temperature range, the spray water flux has the most effect on the heat transfer coefficient. Moreover, the temperature of sprayed water does not have a large influence on the heat transfer coefficient [4].

In the lower part of the secondary cooling zone, heat transfer is preferred mainly by radiation and by roll contact. Therefore, it should be considered that the oxide scales generated on the surface of the strand could cause a thermal resistance in this zone [5].

In this study, the mathematical model has been established on the basis of the technical conditions of the slab caster in the continuous casting unit of Mobarakeh Steel Company. In this model, steel heat capacity and steel thermal conductivity were considered as functions of steel temperature and chemical composition. Considering these functions, the governing equation is a non-linear equation. In this study the equation is solved in non-linear state. This model is also capable of predicting the temperature distribution, including the solidus and liquidus isotherm which defines the solid shell and mushy zone, respectively, as a function of section size, pouring temperature, steel composition, casting speed, mold length and spray conditions.

Mathematical modeling

Figure 2 shows the different regions of the continuous casting machine and the model considered for physical simulation of the caster. A typical method of modeling the strand thermal condition is shown in this figure. The mathematical model is applied to slices of strand that start at the meniscus and travel through the machine at the casting speed. New slices are generated periodically. A sufficient number of slices exist in each cooling zone to give an accurate representation of the thermal condition in each zone. In this model, only a quarter of the strand is considered due to the symmetry of the heat flow conditions (Figure 3).

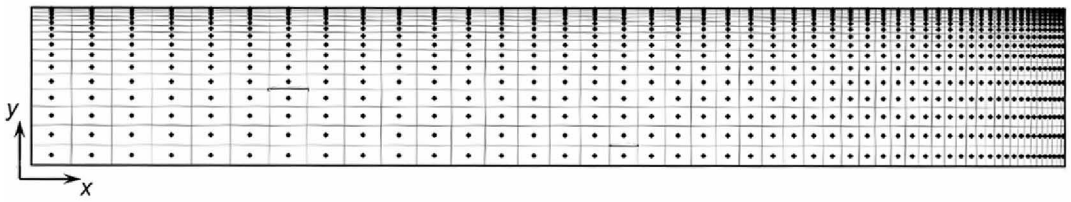

Fig. 3. A symmetric quarter of strand width section with physical coordinate.

Assumptions

The following assumptions are made to simplify the mathematical model [6]:

-Conduction can take place only in the transverse directions.

-Forced convective heat flow in the liquid pool is considered by defining an effective liquid thermal conductivity as:

$$K_{eff} = 7 \cdot K_l \tag{1}$$

-The density of steel is constant, but specific heat capacity and heat conductivity of steel are functions of temperature and chemical composition and therefore not constant.

Model formulation

The energy conservation equation can be written as [7]:

$$\frac{\partial}{\partial t}(\rho H)+\frac{\partial}{\partial x}(\rho u H)+\frac{\partial}{\partial y}(\rho v H)+\frac{\partial}{\partial}(\rho w H)=\frac{\partial}{\partial x}\left(k_{eff}\frac{\partial T}{\partial x}\right)+\frac{\partial}{\partial y}\left(k_{eff}\frac{\partial T}{\partial y}\right)+\frac{\partial}{\partial z}\left(k_{eff}\frac{\partial T}{\partial z}\right) \tag{2}$$

To simplify the equation, a transformation as $\zeta = z - wt$ is used. Therefore this is:

$$\frac{\partial H_s}{\partial t}=\frac{\partial}{\partial x}\left(\alpha\frac{\partial H_s}{\partial x}\right)+\frac{\partial}{\partial y}\left(\alpha\frac{\partial H_s}{\partial y}\right)-\frac{\partial H_l}{\partial t}+\frac{q^0}{\rho};\quad H=H(x,y,\zeta,t);\quad H=H_s+H_l \tag{3}$$

In order to solve the governing equation, it is necessary to transform the physical domain into a computational domain. In general, this sort of transformation is used, and leads to a uniformly spaced grid in the computational domain but the points in physical domain may be unequally spaced. The original partial differential equation is transformed from physical coordinates (x, y) to computational coordinates (ξ, η) by applying the chain rule of partial derivatives.

$$\frac{\partial}{\partial t}\left(\frac{H_s}{J}\right)=\frac{\partial}{\partial\xi}\left(\alpha\frac{\partial H_s}{\partial\xi}\frac{\xi_x}{\eta_y}\right)+\frac{\partial}{\partial\eta}\left(\alpha\frac{\partial H_s}{\partial\eta}\frac{\eta_y}{\xi_x}\right)+\frac{S}{J}; \tag{4}$$

$$S=-\frac{\partial H_l}{\partial t}+\frac{q^\circ}{\rho};\quad J=\xi_x\eta_y$$

In the above equations "S" is a term for heat source due to the metal phase transformation (liquid to solid). In order to establish the region of phase change, the latent heat contribution is specified as a function of temperature i.e. [8]:

$$H_l = f_l \cdot L_f \tag{5}$$

Where L_f is the latent heat of the phase change and the liquid fraction (f_l) is computed by:

$$f_l=\begin{cases}1 & when \quad T \ge T_{liq.}\\ \dfrac{T-T_{sol.}}{T_{liq.}-T_{sol.}} & when \quad T_{liq.} \ge T \ge T_{sol.}\\ 0 & when \quad T \le T_{sol.}\end{cases} \tag{6}$$

A typical 2D cartesian control volume is shown in Figure 4. This C.V contains a central node (P) with four neighborhood points (E, W, N, and S). The integral form of equation (4) is obtained on the control volume by the finite volume method [9,10]:

$$\mathbf{a_P} H_{sP} = \mathbf{a_E} H_{sE} + \mathbf{a_W} H_{sW} + \mathbf{a_N} H_{sN} + \mathbf{a_S} H_{sS} + \mathbf{b} \tag{7}$$

$$a_P = a_W + a_E + a_S + a_N + a_P^\circ$$

$$\mathbf{a_E}=\frac{\alpha_e\Delta\eta}{\Delta\xi}\left(\frac{\xi_x}{\eta_y}\right)_e \qquad \mathbf{a_W}=\frac{\alpha_w\Delta\eta}{\Delta\xi}\left(\frac{\xi_x}{\eta_y}\right)_w$$

$$\mathbf{a_N}=\frac{\alpha_n\Delta\xi}{\Delta\eta}\left(\frac{\eta_y}{\xi_x}\right)_n \qquad \mathbf{a_S}=\frac{\alpha_s\Delta\xi}{\Delta\eta}\left(\frac{\eta_y}{\xi_x}\right)_s$$

$$\mathbf{a_P^o}=\frac{\Delta\xi\cdot\Delta\eta}{\Delta t\cdot J_P}$$

$$\mathbf{b} = a_P^\circ(H_{sP}^{\ o} + H_{lP}^{\ o} - H_{lP}) + \frac{\Delta\xi\cdot\Delta\eta}{\rho J_P}q^o \tag{8}$$

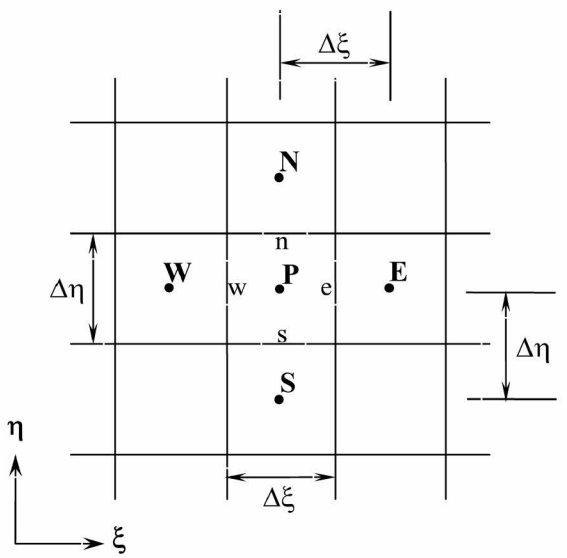

Fig. 4. A typical control volume and the notation used for a Cartesian 2D grid [9].

To approximate the variable values on the surface of the control volume, the Quadratic Upwind Interpolation (QUICK) algorithm is used [9]. In the QUICK scheme, the variable profile between two points approximated by a parabola instead of a

straight line (Figure 5), on a uniform Cartesian grid leads to [9]:

$$\phi_e = \frac{6}{8}\phi_P + \frac{3}{8}\phi_E - \frac{1}{8}\phi_W \quad (9)$$

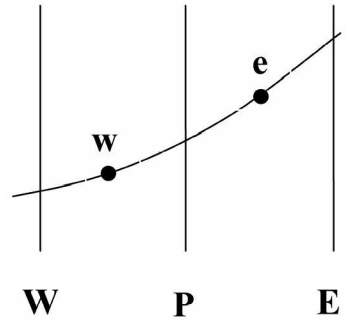

Fig. 5. Approximation of gradients at cell faces [9].

Boundary conditions

To solve the above equation, the boundary conditions are needed for different regions include the mold, water spray cooling, and air cooling. Figure 6 shows some machine cooling layouts while the technical information belonging to each zone is shown in Table 2. A general form of the boundary condition can be expressed through an equation (10), in which the heat transfer coefficient, h, is estimated for different cooling zones.

$$-k\frac{\partial T}{\partial n}|_b = h(T_b - T_{water}) \quad (10)$$

To determine the temperature of the boundaries, the discretion of the $\frac{\partial T}{\partial n}|_b$ on boundary points is required. According to the QUICK scheme $\frac{\partial T}{\partial n}|_b$ could be calculated by the following correlation [10]:

$$\left.\frac{\partial T}{\partial n}\right|_b = \frac{8T_b - 9T_P + T_W}{3\Delta n} \quad (11)$$

Therefore, as seen in equation (10), finding the heat transfer coefficient for different regions such as: mold, water spray, and air cooling is necessary.

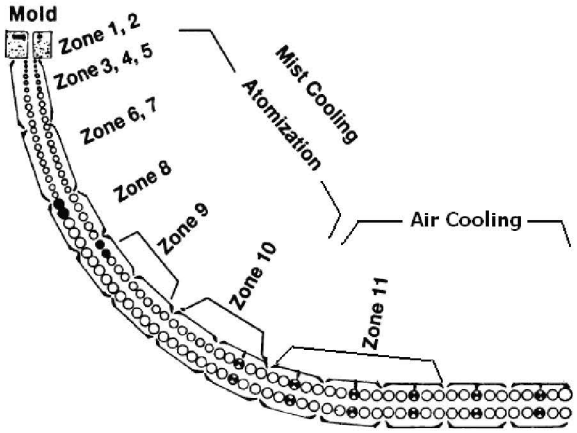

Fig. 6. Secondary cooling of the slab caster.

In the mold, several thermal resistance layers exist between the steel shell surface and the recirculation water. All the thermal resistances in the mold are shown in Figure 7. The effective thermal resistance of the water channel is estimated from the water channel heat transfer coefficient, thermal conductivity and the thickness of scale deposits on the surface of the cooling-water channel [11]:

$$r_{water} = \left(\frac{d_{scale}}{k_{scale}} + \frac{1}{h_w}\right) \quad (12)$$

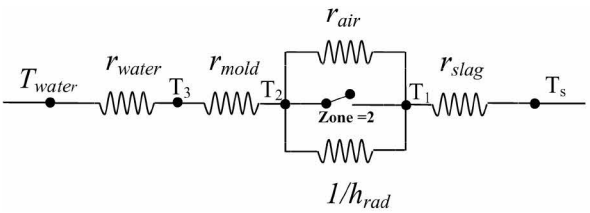

Fig. 7. Thermal resistances existing between the shell surface and water channel in the mold.

Table 2. Secondary cooling zones variables.

No. Zone	Length zone (m)	Segment	Number of spray nozzles	Water flow rate (m^3/sec)	Number roll in zone	Roll radius (m)
1	0.439	-	-			
2	0.220	-	-			
3	0.303	-	30	0.003975	-	-
4	0.925	0	38	0.004967	5	0.140
5	1.470	0	38	0.004842	6	0.200
6	1.475	1	10	0.004858	5	0.250
7	1.725	2	10	0.003975	5	0.300
8	1.725	3	10	0.003733	5	0.300
9	3.950	4,5	20	0.005667	10	0.350
10	5.200	Roll 37-47	22	0.006483	11	0.380,0.440
11	9.400	Roll 48-63	-	Air cooling	16	0.440

The heat transfer coefficient between the water and the side walls of the water channel (h_w) is calculated assuming a turbulent flow through an equivalent-diameter pipe (D) using the empirical correlation of Sleicher and Reusse [11]:

$$h_w = \frac{k_{water}}{D}\left(5 + 0.015\,\mathrm{Re}^{c_1}\,\mathrm{Pr}^{c_2}\right) \quad (13)$$

$$c_1 = 0.88 - 0.24/(4+\mathrm{Pr}); \quad c_2 = 0.333 + 0.5^{\,-0.6\,\mathrm{Pr}}$$

Other thermal resistances shown in Fig 7 can be calculated by the following correlations [11]:

$$r_{mold} = \frac{d_{mold}}{k_{mold}}; \qquad r_{slag} = \frac{d_{slag}}{k_{slag}}; \quad r_{air} = \frac{d_{air}}{k_{air}}; \quad (14)$$

Which d_{slag} can be found from the powder consumption per mass of product ($M_{slag\ (kg/ton)}$):

$$d_{slag} = \frac{M_{slag} \times \rho_{steel}}{\rho_{slag}} \times \frac{W \times N}{2(W+N)} \quad (15)$$

Also, d_{air} includes a gap due to shrinkage of the steel shell, which can be calculated by the thermal linear expansion relation of steel using following correlation for each control volume:

$$\Delta l = \lambda \cdot l \cdot \Delta T \quad (16)$$

Where, λ is linear thermal expansion coefficient of steel and l is length of each control volume.

Moreover, the heat transfer coefficient due to radiation is calculated by:

$$h_{rad} = \varepsilon\sigma\left(T_1^2 + T_2^2\right)\left(T_1 + T_2\right) \quad (17)$$

Heat transfer mechanisms in the spray cooling zones below the mold are defined in Figure 8. The heat extraction due to the water sprays is a function of the water flux. The relationship between the rate of heat extraction by the water sprays and the spray variables has been established in a number of experimental studies. One of the most widely used relations has been presented by Nozaki's [12]:

$$h_{spray} = 0.3925 \times Q_{water}^{0.55} \times \left(1 - 0.0075 \times T_{water}\right); \quad (18)$$

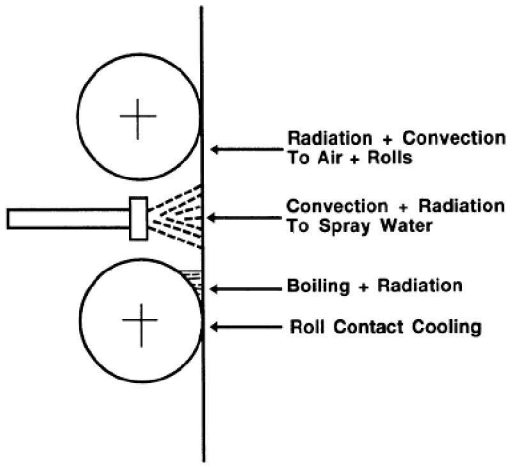

Fig. 8. Heat transfer mechanisms in the secondary cooling zones [12].

Due to the high temperature of the strand surface and the exposure of water to the surface, an oxide scale is produced on the surface of the strand. Despite the low thickness, the scale can have an important role in the heat transfer control. Therefore, the effective heat transfer coefficient should be considered as [12]:

$$h_{eff} = \frac{1}{\frac{\delta_{sc}}{k_{sc}} + \frac{1}{h_{spray}}} \quad (19)$$

It has already been mentioned that the cooling of the strand in the lower part of the secondary cooling zone is mainly done by radiation [12]. Therefore, the equation for the heat transfer coefficient is given as follows:

$$h_{rad} = \varepsilon\sigma\left(T_s^2 + T_{am.}^2\right)\left(T_s + T_{am.}\right) \quad (20)$$

Besides the radiation, heat transfer is also achieved by natural convections, but this part is rather small and can be neglected in comparison to radiation cooling.

The symmetrical boundary condition has been considered for midplanes as follows:

$$x = 0., \quad -k\frac{\partial T}{\partial x} = 0$$
$$y = 0., \quad -k\frac{\partial T}{\partial y} = 0 \quad (21)$$

Computation and verification

The algebraic equation of the boundary conditions has been solved with a Tridiagonal Matrix Algorithm (TDMA) solver [13]. As seen in equations (7) and (8), to solve the algebraic equation, it is necessary to know the latent enthalpy in a new time step (H_l). To update the amount of the latent enthalpy an iterative solution is used for each time step:

$$H_{lP}^{k+1} = H_{lP}^{k} + H_{sP}^{k} - H_{sP}^{k+1} \quad (22)$$

As seen in the above equation, by using the sensitive enthalpy that has been obtained by solving the energy equation (H_{sP}^{k+1}), latent enthalpy could be updated in the k+1th inner iteration in each time step to achieve a certain convergence. The calculation mentioned has been programmed in the FORTRAN language. The mathematic simulation starts by setting the initial steel temperature at the pouring temperature. Input parameters, in Table 3, in the standard cases are verified by the measured temperatures on the shell surface of the strand.

Equilibrium lever-rule calculations are performed on a Fe-C phase diagram in order to calculate steel phase fractions. By this means, phase field lines are specified as simple linear functions of carbon equivalent content. The carbon of the steel is applied as the carbon equivalent content that is calculated by the following correlation [14]:

wt%CE=wt%C+ 0.04(wt%Mn)-0.14(wt%Si)-
0.04 (wt%Cr)-0.1(wt%Mo)-
0.24(wt%Ti)+0.1(wt%Cu)

For a 0.16%C, 1.3%Mn, 0.5%Si, 0.05%Cr, 0.03%Mo and 0.01%Ti plain carbon steel, the carbon equivalent percentage calculated as 0.135 and also the equilibrium phase diagram model calculates $T_{liq.}$=1528 °C, T_{sol}= 1494 °C. The solid fraction-

temperature curve in the mushy zone obtained from the model is shown in Figure 9. As seen in this figure the relation between temperature and solid fraction of steel in the mushy zone is non-linear.

Solidified shell thickness is one of the most important calculated parameters in the model, and the influence of the grid spacing on this parameter should be considered. The influence of the grid spacing on the solidified shell thickness, in exit point of the mold, is shown in Table 4. The thickness amounts in width and narrow sides are presented in this table. It is clear from Table 4 that when grid spacing is reduced, solidified thicknesses are changed and they are stable in a narrow limit with reduction of grid spacing lower than a certain limit. It can be concluded that the solidified shell thickness is independent of the mesh size with the reduction of grid spacing lower than a certain limit.

The mold zone is a complex and important area in continuous casting machine. The solid shell growth in this zone is complicated and the results of this study are compared to those of some other researchers. The comparison between the results of the model in this study and experimental measurement by some other researchers is shown in Figure 10. The figure shows the variation of growth of the solid shell thickness on the ingot for low carbon steel (0.06% C). It is clear that the results from numerical solution in this study have a very good compatibility with those of three 3-D model of Thomas and experimental measurement of Alberny and co-worker.

Table 3. Input data for standard conditions.

Carbon equivalent content, CE pct	0.132	pct
Steel density, ρ	7500	kg/m^3
Steel emissivity, ε	0.8	
Mold copper plates thickness	0.043×0.030	m×m
Total mold length	0.704	m
Mold copper plates width	2.220×0.215	m×m
Scale thickness on the surface of mold cold face	0.00001	m
Mold conductivity, k_{mold}	315	W/mK
Mold powder conductivity, k_{slag}	1.27	W/mK
Air conductivity, k_{air}	0.083	W/mK
Mold powder density, ρ_{slag}	0.650	kg/m^3
Mold powder consumption rate, M_{slag}	0.8	kg/ton steel
Casting speed, V_c	0.0167	m/sec
Pour temperature, T_{in}	1546	°C
Liquidus temperature, $T_{liq.}$	1528.6	°C
Solidus temperature, $T_{sol.}$	1494	°C
Working mold length	0.659	m
Slab geometry, $W \times N$	1.250×0.203	m×m
Scale conductivity on the surface of slab, k_{sc}	0.5	W/mK
Scale conductivity on the surface of mold, k_{scale}	1.0	W/mK
Water channel geometry, large & small plates	25×5×29 & 22×5×26	mm^3
Average cooling water temperature in the mold	28	°C
Water flow rate entering the mold small plate,	0.0061	m^3/sec
Water flow rate entering the mold large plate,	0.0553	m^3/sec
Latent heat of the steel phase change, L_f	272140	J/kg
Water conductivity, k_{water}	0.615	W/mK
Steel specific heat capacity[11], C_p	$\begin{cases} C_p = 456 + 0.376 * T(^oC) & T \le 500 \\ C_p = 268 + 0.836 * T(^oC) & 500 \le T \le 700 \\ C_p = 1431 & 700 \le T \le 750 \\ C_p = 3849 - 3.766 * T(^oC) & 750 \le T \le 850 \\ C_p = 648 & 850 \le T \le 1100 \\ C_p = 268 + 0.334 * T(^oC) & 1100 \le T \le T_{sol} \\ C_p = 772 & T_{sol} \le T \le T_{liq} \\ C_p = 787 & T \ge T_{liq} \end{cases}$	J/kgK
Steel conductivity, k_{steel}	$f_l * k_{liq} + (1-f_l) * k_{sol}$	W/mK
Solid steel conductivity, k_{sol}	33.0	W/mK
Effective molten steel conductivity, k_{liq}	7*43.0	W/mK
Scale thickness on the surface of slab, δ_{sc}	0.001	m

Table 4. Effect of mesh size on the shell thickness at mold exit.

Grid system # $n_x \times n_y$	Shell thickness at middle of wide face (m)	Shell thickness at middle of narrow face (m)
25×10	0.0145	0.0111
25×15	0.0135	0.0110
50×15	0.0136	0.0118
50×20	0.0133	0.0119
100×20	0.0136	0.0117
100×30	0.0131	0.0117

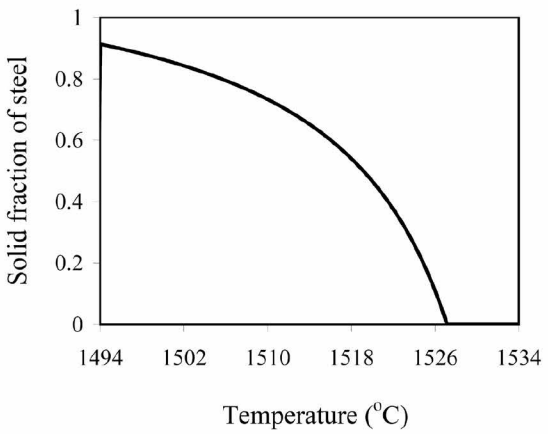

Fig. 9. Phase fraction variation with temperature in mushy zone.

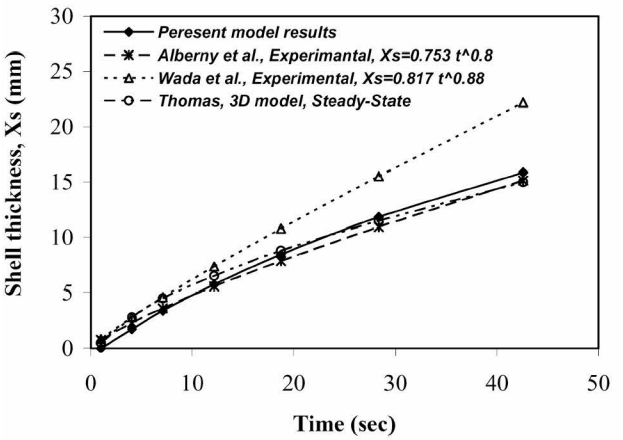

Fig. 10. Comparison between model results and other references.

Results and discussion

The calculated surface temperatures of a slab, for the Table 3 conditions as a function of the distance below the meniscus, are presented in Figure 11. This figure shows the calculated surface temperatures at the centers of the wide and narrow faces and at the corners of the slab caster. The central areas of the wide faces are cooled one-dimensionally, whereas the slab corners are subject to 2-D cooling. The slab corners can therefore become significantly colder than other parts of the inner wide face. At the beginning of straightening, the slab corner temperature is 230 °C less than the temperature at the center of the wide face. Control of corner cooling is critical for much of continuously cast products. The slab corners tend to have meniscus marks, which act as stress risers. A combination of temperature, stress risers and a low ductility region in the 700-900 °C temperature range during the straightening process often leads to cracks in the corners. One way to increase the corner temperature is to widen the strip of unsprayed strand at the corner. However, as the non-sprayed strip is widened, a hot spot will develop between the colder corner and the sprayed area. Thus, the design must be in a way to ensure that it does not cause other quality problems. Also, as seen in Figure 11, the intensity of heat transfer of mist spray cooling is less than cooling in the lower part of the mold for all of the curves, because of this, the model predicts a 200 °C reheating of the slab surface on leaving the mold. A similar situation also exists in water spray cooling and air cooling regions on the surface of the wide face slab.

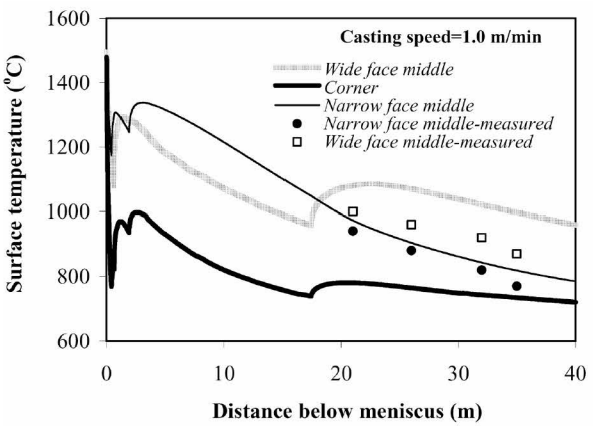

Fig. 11. Predicted surface temperature of strand.

Figure 12 shows the solidified shell thickness profiles of both the narrow and wide faces of the slab. This figure shows a sudden change of slope at the beginning of the solidified shell growth curve. It is indicated that the rate of solidified shell growth is clearly high in the mold region. Figure 13 shows a set of data of the local heat flux density along the length of the mold [15]. There is a maximum of heat flux density somewhat below the meniscus. Downward, the heat flux density usually decreases. If the air gap

between the mold and strand approximately has uniform thickness, or it increases uniformly in the downward direction, the heat flux density along the length of the mold continuously decreases.

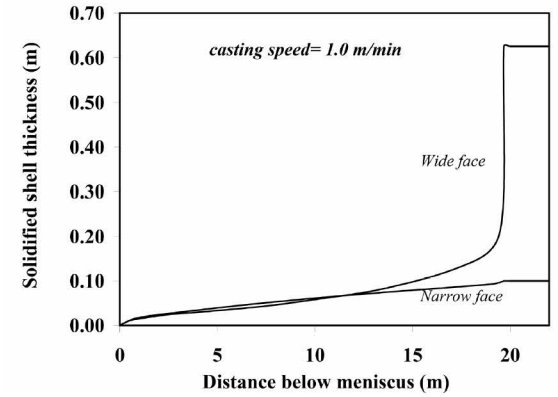

Fig. 12. Predicted solidified shell thickness.

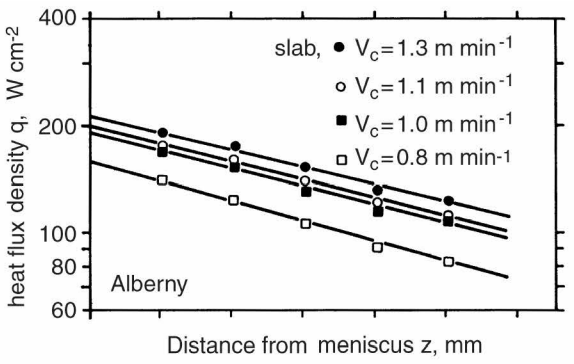

Fig. 13. Heat flux density distribution along the length of the mold.

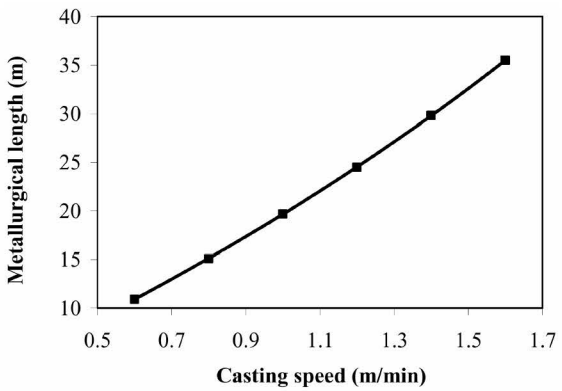

Fig. 14. Effect of casting speed on the pool depth.

The casting speed is the most effective parameter in changing the position of the solidified shell thickness profiles. The relation of the "metallurgical length" (maximum length of the liquid pool) with the casting speed is shown in Figure 14. Increase in casting speed decreases the holding time of the slab in the secondary cooling zones and increases the length of the liquid core. Therefore, casting speed is the most important factor in controlling mold heat extraction. The solidified shell thickness as a function of the casting speed of both wide face and narrow face of the strand are shown in Figure 15. Since, a lower casting speed provides more time for the heat to be extracted from the shell, the shell thickness increases. Moreover, the shell thickness in the initial solidification stage decreases at the high casting speed, as shown in Figure 15, which often easily causes the breakout of strand. Therefore, to prevent this unfavorable defect, the casting speed is limited. It should be mentioned that steel composition and slab width in comparison to casting speed has no significant effect on the shell thickness. As seen in this figure, solidified shell thickness for wide face is higher than it is for narrow face. This is because of the different air gap sizes between mold powder and mold wall in both wide and narrow faces. The air gap size along the length of the mold is predicted by the model for both faces in Figure 16. As seen in this figure, total shrinkage value in narrow face is more than wide face as expected because width size of slab is much larger than thickness size in cross section of strand. Furthermore, this phenomenon could change interfacial gap temperature for different layers.

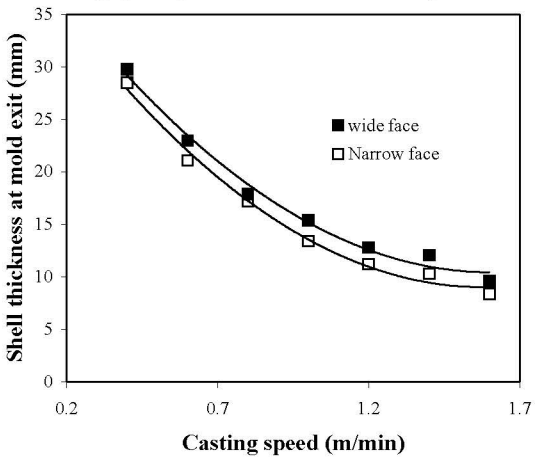

Fig. 15. Effect of casting speed on shell thickness.

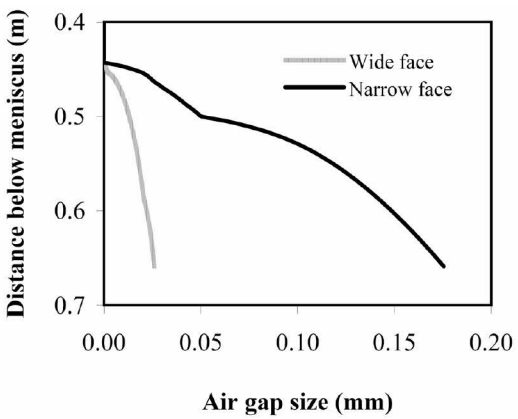

Fig. 16. Air gap size along the mold.

Heat transfer in the mold is governed by these three resistances: the casting-mold interface, the mold wall, and the mold-cooling water interface. Although, thermal resistance due to the air gap

should also be considered while the amount of air gap thermal resistance is usually quite large compared to the other resistances especially for the lower portion of the mold. Temperatures of three points: slag layer/mold wall interface (T_1), mold wall (T_2), and water channel wall (T_3) as shown in Figure 7 are predicted by the model. Since, the heat flux for steady state conditions will be constant and independent of distance: (23)

$$q' = \frac{T_s - T_{water}}{r_{total}} = \frac{T_s - T_1}{r_{slag}} = \frac{T_s - T_2}{r_{slag} + \left(\frac{r_{air} \cdot r_{rad}}{r_{air} + r_{rad}}\right)} = \frac{T_s - T_3}{r_{slag} + \left(\frac{r_{air} \cdot r_{rad}}{r_{air} + r_{rad}}\right) + r_{mold}}$$

The above relation represents three equations for the three unknowns, T_1, T_2, and T_3. The results of the model predictions are shown in Figure 17(a) and Figure 17(b). As seen in these figures, the existence of the air gap between the shell surface and mold wall causes the T_1 to increase both in wide and narrow faces of strand. Since the air gap thickness in the narrow face is larger than the wide face, T_1 in the narrow face is much higher than in the wide face. Therefore, the pattern of heat removal in the mold is dependent largely upon the dynamics of gap formation. It causes temperature difference to exist in solidified shell and has a strong influence on transverse cracks generation in the mold region.

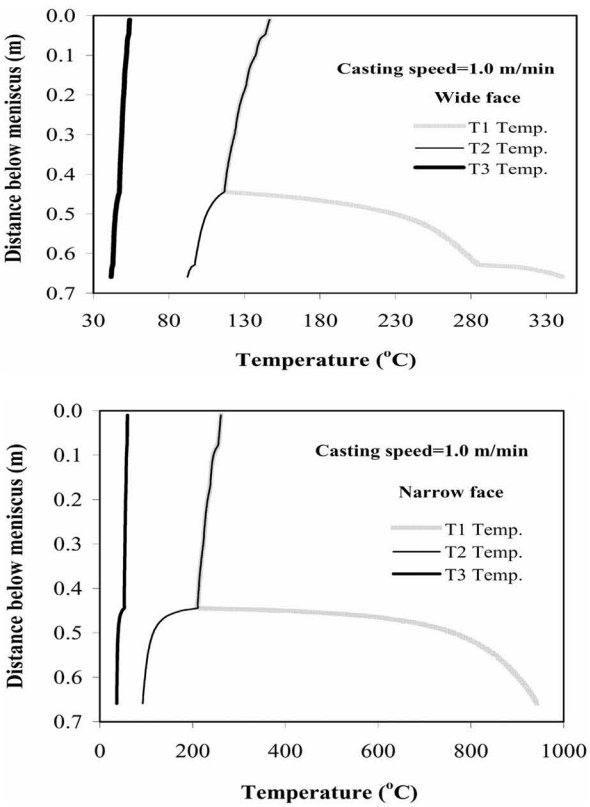

Fig. 17. Predicted temperatures for T_1, T_2 and T_3 points in Fig 7 -(a) wide face and (b) narrow face (T_1=slag layer/mold wall interface temperature, T_2=mold wall temperature, and T_3=water channel wall temperature).

The effect of the amount of superheat temperature of the molten steel, entering the mold, on the solidified shell thickness is shown in Figure 18. At first, with increasing the superheat temperature, the superheat flux will increase and therefore, the solidification rate decreases. This, in turn, reduces the thickness of the steel shell. On the other hand, by increasing the superheat temperature, the driving force for the heat transfer will increase. Therefore, as seen in Figure 18, the influence of the superheat temperature is insignificant to shell growth, especially in the wide face of the strand. Low superheat, near liquidus temperature, is beneficial to continuous casting. Internal quality is improved as the equated zone is made significantly larger. Therefore, a more desirable structure with greater resistance to halfway cracks is produced. Centerline segregation and porosity are also reduced or eliminated.

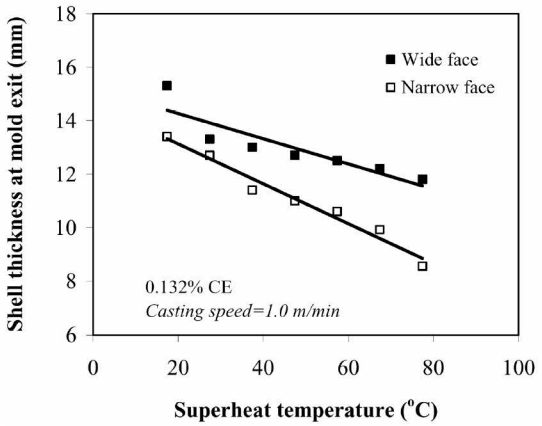

Fig. 18. Effect of steel superheat temperature on the shell thickness at mold exit.

Conclusions

1- A finite volume heat transfer and solidification model has been formulated to predict the temperature field and liquid pool position in the continuous casting process under different conditions. This has been verified with the temperature measurement of slab surface.

2- Casting speed is the most effective parameter on mold heat removal. Therefore, it is the most important factor in controlling solidified shell thickness and slab temperature.

3- Since, the air gap size in narrow face of mold is higher than the wide face, the breakout of strand often occurs in the narrow face.

4- Air gap existing in the casting-mold interface causes a large thermal resistance for heat transfer from the solidified shell to the mold. Therefore, it has a strong influence on product quality and casting problems, especially for the narrow face of strand.

5- High superheat temperature may cause breakouts at the mold exit, especially for the narrow face, so it should be exactly kept at a low level.

List of symbols

d_{air}: Air gap thickness (m)
d_{mold}: Copper mold thickness (m)
d_{slag}: Slag layer thickness (m)
f_s: Solid steel fraction
h_{rad}: Heat transfer coefficient due to radiation (W/m^2K)
h_{spray}: Heat transfer coefficient due to water spray ($kW/m^{2o}C$)
h_w: Heat transfer coefficient due to water circulation in the mold (W/m^2K)
H: Total enthalpy (j/kg)
H_l: Steel Latent enthalpy (j/kg)
H_s: Steel sensitive enthalpy (j/kg)
k: Steel thermal conductivity (W/mK)
k_{air}: Air thermal conductivity(W/mK)
k_{mold}: Copper mold thermal conductivity (W/mK)
k_{sc}: Oxide scale thermal conductivity created on the surface of strand(W/mK)
k_{scale}: Oxide scale thermal conductivity in the water channel (W/mK)
k_{slag}: Mold powder thermal conductivity (W/mK)
k_{water}: Water thermal conductivity (W/mK)
L_f: Latent heat of steel (j/kg)
N: Slab thickness (m)
Q_{water}: Water flow rate in spray zone (lit/m^2sec)
r_{rad}: Thermal resistance due to radiation (Ω)
r_{air}: Thermal resistance due to air gap(Ω)
r_{mold}: Thermal resistance due to cupper mold (Ω)
r_{slag}: Thermal resistance due to slag layer (Ω)
r_{water}: Thermal resistance due to water circulation channel (Ω)
T: Steel temperature (^oK)
T_b: Steel temperature on the domain boundary's (^oK)
T_{water}: Mean water temperature in the mold channel (^oK)
W: Slab width (m)
v_c: Casting speed (m/sec)
α: Steel thermal diffusivity (m^2/sec)
δ_{sc}: Oxide scale thickness (m)
ε: Mean surface emissivities=0.8
ρ: Steel density (kg/m^3)
σ: Stefan Boltzman constant $=5.67\times10^{-8}$ (W/m^2K^4)

Refrences

[1] C. A. Santos, J. A. Spim, and A. Garcia, Eng. Appl Artif. Intel., 16 (2003), 511.
[2] J. Cho, H. Shibata and T. Emi, ISIJ Int., 38 (1998), 440.
[3] A. W. Cramb, The Making, Shaping and Treating of Steel, 11th Edition Casting Volume, The AISE Steel Foundation, Pittsburgh Pa.,Chapter 4, (2003), 3.
[4] B. G. Thomas and L. Zhang, ISIJ Int., 41 (2001), 1181.
[5] S. H. Seyedein and M. Hasan, Can. Metall. Quart , 37 (1998), 213.
[6] H. Wang, G. Li, and J. Wang, Journal of University of Science and Technology Beijing, 11 (2004), 18.
[7] A. Bejan, Convection Heat Transfer, John Wiley & Sons, Durham, North Carolina, (1984), 18.
[8] X. K. Lan, and J. M. Khodadadi, Int. J. Heat Mass Trans., 44 (2001), 953.
[9] J. H. Ferziger and M. Peric, Computational Methods for Fluid Dynamics, Springer, (1997), 74.
[10] W. J. Minkowycz, E. M. Sparrow, and G. E. Schnrider, Handbook of Numerical Heat Transfer, John Wiley & Sons, Inc , USA, (1988), 117.
[11] Y. Meng and B. G. Thomas, Metall. Mater. Trans. B, 34 (2003), 685.
[12] J. K. Brimacombe, I. V. Samarasekera and J. E. Lait, Continuous Casting Vol. 2, BookCrafters Inc , USA, (1993), 140.
[13] D. A. Anderson, J. C. Tannehill and R. H. Pletcher, Computational Fluid Mechanics and Heat Transfer, Hemisphere, USA, (1984), 98.
[14] A. Yamauchi, T. Emi, and S. Seetharaman, ISIJ Int., 42 (2002), 1084.
[15] R. Alberny, A. Leclerdq, D. Amaury and M. Lahousse, Rev. Metall., 73 (1976), 545.